FRACTURE STUDIES ON SYNTHETIC FIBER REINFORCED CELLULAR CONCRETE USING ACOUSTIC EMISSION TECHNIQUE

Abdur Rasheed, M[1], Suriya Prakash. S[2], Gangadharan Raju[3], Yuma Kawasaki[4]

[1] Research Scholar, Email: ce13m15p100001@iith.ac.in
[2]Associate Professor and Corresponding Author, Email: suriyap@iith.ac.in
[3]Assistant Professor, Email: gangadharanr@iith.ac.in
Department of Mechanical and Aerospace Engineering, IIT-Hyderabad, Telangana, India
[4]Associate Professor, Email: yuma-k@fc.ritsumei.ac.jp
Department of Civil Engineering, Ritsumeikan University, Shiga, Japan

ABSTRACT

Cellular lightweight concrete (CLC) is increasingly used for low strength non-structural and structural applications. The effects of synthetic fiber reinforcement on the fracture behavior of CLC is investigated. In particular, acoustic emission (AE) technique is employed to study the influence of macro (structural), micro polyolefin synthetic fibers and their combinations on the fracture behavior of CLC beams. Notched fiber reinforced CLC beams were tested to study the crack initiation and propagation characteristics using AE sensors. Different AE parameters are correlated with the crack growth and damage accumulation. An attempt has been made to correlate the crack mouth opening displacement (CMOD) with the number of AE hits. The variation of cumulative acoustic energy release of the cracks is studied with respect to applied load and CMOD. Three dimensional source location of cracks is carried out based on the AE events picked by the sensors bonded to the CLC specimens. The analysis of AE results indicates that the crack source location identification from AE is consistent with the actual crack development. Analysis of AE signals reveal that the CLC matrix cracking produces signals with less number of hits that lie in the notched plane in bending. Moreover, the signals from the post peak regime correspond to more number of hits which tend to be scattered around the plane of notch due to the fiber pull out.

Keywords: Acoustic Emission; Crack propagation; Fracture Behavior; Health Monitoring; Hybrid Fibers; Non-destructive testing; Polyolefin fibers;

1. INTRODUCTION

Cellular lightweight concrete (CLC) is increasingly used in various low strength structural and non-structural applications due to its properties like low density, termite resistance, high thermal and acoustic insulation [1]. CLC is widely used in infill masonry construction, soil stabilisation, solid fills for hollow aluminium doors and window frames, thermal insulation on roof slabs, and in tunnel linings [2], [3]. Moreover, CLC can be classified as sustainable and green building material due to the usage of high volume of fly ash during the manufacturing process [4]. The low carbon footprint involved in manufacture of CLC makes it an eco-friendly building material. However, the low tensile strength and brittle nature of CLC raises concerns when subjected to flexure, tensile and shear loading and limits its different applications.

Usage of synthetic fiber as a reinforcement in cellular concrete has increased in the recent years due to its ability to transform the brittle behavior of CLC into ductile under various modes of testing such as compression, flexure, tension, shear and impact [5]. Fiber reinforced CLC (FRCLC) is one such special concrete which has enhanced toughness, better composite behavior, durability and impact resistance compared to their unreinforced counterpart [6], [7]. Improvement of mechanical properties of high performance concrete by addition of synthetic fiber reinforcement has been confirmed by many researchers [8]–[12]. Although steel fibers have superior mechanical properties compared to that of synthetic fibers, they decrease the workability and creates a balling effect at higher dosage. On the other hand, structural synthetic fibers, being non-corrosive and malleable, have gained attention in the recent years. They are also used for reinforcing cementitious materials to control the crack propagation and improve the overall structural performance [8], [9]. Synthetic plastic fibers used in this study are not green and a sustainable mateiral. Use of natural fibers may be a sustainable option. Nevertheless, the fiber volume fraction used in this study is very minimum of up to 0.55%.

This is relatively a low proportion compared to the volume of the matrix. In addition, recycled plastic wastes can also be used as fiber reinforcement in CLC. Besides, the synthetic fibers used in this study have well defined mechanical properties, which the natural fibers and other recycled fibers lack. Therefore, to reduce the variability in the experimental program, synthetic fibers with relatively low dosages are used. Polyolefin fibers used in this study comes under the category of synthetic fibers. They are manufactured in two different types (a) Mono-filament and (b) fibrillated. Monofilament fibers have constant cross sectional area along its length. Fibrillated fibers are produced as films or tapes which can transform like net when mixed with concrete. Synthetic Polyolefin fibers can also be classified as micro or macro (structural) fibers. Micro-synthetic fibers are typically 12 mm long and 0.018 mm in diameter. Macro ones are typically longer (40 to 50 mm) and larger (0.3 to 1.5 mm) in size. Better bonding characteristics is now possible by the virtue of surface improvement on the fiber. Low density, better corrosion resistance and chemical inertness makes synthetic fibers a better choice for FRC when compared to the steel fibers. However, the low modulus of elasticity of synthetic fibers restricts them to be used as primary reinforcement. Nevertheless, these fibers can be used for special applications like cold storage walls, slab on-grade, ballast less subgrade track, tunnel linings and non-load bearing precast partition walls in high rise framed structures/ load bearing walls of appropriate thickness in low rise buildings [13]. Therefore, it is important to understand the effect of fiber reinforcement on the fracture behavior of CLC to increase its wide spread usage.

Fracture parameters for CLC has been investigated in the past [14]. Indirect tensile strength, strain softening and fracture energy of different types of aerated autoclaved concrete (AAC) has also been reported [15]. Crack nucleation is a phenomenon where cracks at micro scale coalesce to from a macro crack, which eventually leads to the failure of concrete under flexure. The three dimensional region where this process happens is referred to as fracture

process zone (FPZ) [16]. In particular, acoustic emission (AE) technique is used to quantitatively assess the crack growth in structural elements by correlating it with the AE hits encountered. It can be argued that the pores in the cellular concrete can hinder the propagation of elastic waves emanating from the crack source, thereby weakening the signal strength. This is true in case of porous concrete materials where the matrix media is predominantly disconnected. Whereas in cellular concrete material, the pore structure is disconnected. This makes the CLC medium continuous and does not hinder the wave propagation.

Attempts have been made in the past to qualitatively define the damage accumulation in concrete using acoustic emission (AE) technique [17]. Berthelot et al. [18] performed frequency analysis on concrete specimens to identify AE events by deducing its spectrum from detected signal. Sause and Stefan [19] modelled AE crack source using finite element modelling approach which calculates the dynamic displacement field during crack formation. Landis and Shah [20] conducted experimental study on flexural behavior of mortar beams to evaluate micro-crack parameters using AE technique. They found that the predominant mode of fracture in micro-cracks of mortar is mode II. Recent study has confirmed that AE activity increases with the amount of steel fiber reinforcement [21]. Qualitative fatigue crack classification on reinforced concrete beams was studied by Noorsuhada et al. [22]. Two indices of AE parameters were used and the relationship indicated the transition of crack mode corresponding to the damage development. Hu et al. [23] conducted fracture tests on notched concrete beams and illustrated that AE technique can be employed effectively to determine the crack propagation until the complete failure of specimen. In addition, they also noted that AE technique could help in obtaining the initial fracture load and unstable load at a slow loading rate. Cracking due to corrosion has been detected and located [24]–[30] using AE technique. Aggelis et al. [31] conducted the shear and tensile fracture test on cementitious materials by

altering the loading equipment. It was observed that different modes of fracture process can be identified using AE technique. Aldahdooh and Bunnori [32] tested reinforced concrete beams under flexure and showed that the initial level of damage was associated with the tensile mode and gradually shifted towards shear mode of failure with increase in damage levels. The test results from AE technique has also been verified by researchers [33]–[35] using digital image correlation (DIC) technique. The focus of this investigation is to understand the fracture behavior of FRCLC under flexure. Notched FRCLC specimen were tested under three-point bending configuration with AE sensors attached on the surfaces. Generally, the AE sensors can range from 5 kHz upto 2000 kHz. Studies from past reveals that for studying normal concrete narrow band sensors are sufficient. However, since the CLC material has been investigated using AE sensors for the first time, the authors wanted to make sure that, any higher frequency wave is not eliminated by the use of only narrow band sensors. Finally, the analysis of the results shows that the average frequency lies in the range of 50kHz to 350kHz. Therefore, usage of two different kind of sensors results in overlap of frequency range of 200kHz with a difference of ±50kHz. Crack formation modes can be distinguished into shear and tensile modes based on the two methods viz., Parameter based method and simplified Green function for moment tensor analysis (SiGMA) procedure [36].

In the recent years, continuous monitoring of structures in-service has been highlighted around the world. Thus, development of non-destructive evaluation (NDE) techniques for the inspection of concrete structures is currently in high demand. Varieties of innovative NDE techniques are actively under development in concrete engineering, which are closely associated with fracture mechanics. Fracture in a material takes place with the release of stored strain energy, which is consumed by nucleating new external surfaces (cracks) and emitting elastic waves. The latter phenomenon is defined as acoustic emission (AE). The elastic waves propagate inside a material and are detected by an AE sensor. By analyzing the detected signals,

more useful information associated with the damage location and extent of internal damage can be assessed successfully. Thus, the AE technique can be a viable non-destructive and reusable tool compared to the conventional mechanical testing for health monitoring. In this way, the authors believe that with proper calibration and in-depth scientific reasoning, AE technique can be an indispensable tool for non-destructive evaluation of new sustainable materials such as fiber reinforced CLC explored in this study.

2. RESEARCH SIGNIFICANCE

Number of investigation in the past have focused on understanding the behavior of fiber reinforced concrete using AE technique. However, the acoustic emission behavior of fiber reinforced CLC has not been adequately investigated in the past. To fill in the existing knowledge gap, the current study aims at the following: (i) study the fracture parameters of fiber reinforced CLC material under flexure, (ii) qualitative analysis of various AE parameters for the corresponding crack initiation and propagation in CLC, (iii) quantification of damage accumulation by studying the crack growth against the cumulative acoustic emission counts and (iv) identification of fracture process zone (FPZ) using AE source location and differentiating the type of failure modes by correlating AE parameters with crack mouth opening displacement (CMOD).

3. EXPERIMENTAL PROGRAM

3.1. Materials

The material ingredients used for casting CLC consisted of ordinary Portland cement (OPC), class F-flyash, potable water and foaming agent (Table 1). Design mix proportions used for achieving a characteristic density of 950 ± 20 kg/m^3 are given in Table 1. Water-binder ratio is kept constant at 0.38, considering the fly ash also acts as binder. Fiber dosage of 5kg/m^3 is

158 kept as the upper value based on the observed stress strain behaviour under compression. For
159 a particular batch of specimen, the amount of fiber is added in addition to control mixture
160 proportion. For instance, the addition of fiber for 0.55% volume fraction is 5kg of fibers per
161 cubic meter of concrete. The volume fraction of fiber is very less compared to the total volume
162 of the mix. Therefore, the impact of addition of fiber in the mix proportion volume was found
163 to be negligible on workability. CLC mix used in this study does not have any aggregates. The
164 mix contained only cement, fly ash, foaming agent, water and different dosages of fibers.
165 Therefore, the mix remained in liquid state even after adding fibers. Patty tests showed the
166 spread was more than 500 mm even at addition of higher fiber dosages of 0.55%. CLC mix
167 used in the study flowed into the moulds like self-compacting concrete and remained
168 unaffected by addition of fibers. It showed equally good mobility into the moulds even after
169 addition of high volume of fiber dosages. Improved workability tests like slump flow test and
170 flowability test on CLC with different fiber dosages would be interesting and are scope for
171 further work.
172 Fly ash procured from national thermal power plant corporation (NTPC) is used in the CLC
173 mix. It had a minimum of 20% of fines for obtaining the optimum strength to weight ratio.
174 Organic content and other impurities in the fly ash were found to be within tolerance limits.
175 Siliceous fly ash of class F is used and its basic chemical composition is provided in Table 2.
176 OPC 53 grade is used in the preparation of CLC mix. For early demolding of CLC blocks, high
177 early strength cements can also be used as suggested by IS 2185 Part 4 [37]. However, it has
178 been observed that slower the hardening rate, the better will be the final quality of CLC blocks.
179 The addition of fly ash serves as an economical substitute for cement, reduces its shrinkage,
180 and slows down the hardening rate of the mix. Keeping in view of all these requirements, OPC
181 is used with the fly ash in the ratio of 1:3.
182

183 **TABLE 1.** List of proportions (kg/m^3) in Design Mix

Component	Cement	Flyash	Water	Foam
Proportion (kg/m^3)	277	715	277	1.4

184

185 **TABLE 2.** Basic chemical composition of Class F fly ash

Component	SiO_2	Al_2O_3	CaO	Fe_2O_3	MgO	Alkalies	Organic impurities
Proportion (%)	50-60	24-27	6-8	10-13	1	1.5	3-4

186

187 Maintaining the stability of foam is essential for achieving the desired density of CLC mix and
188 to have a closed pore structure. Protein hydrolyzed foaming agents impart the desired
189 characteristics to the foam generated. For the purpose of this study, a commercially available
190 foaming agent was used. Foaming agent and water was mixed in a ratio of 1:40 and fed into
191 foam generator to achieve a density of 70g/litre of the pre-formed foam. The volume fraction
192 of foam in the mix is 16% of the total volume. Total volume of the pores in the CLC is 35%.
193 Care has to be taken that the water or foaming agent should not come into contact with
194 oily/waxy agents due its harmful effect on the surface tension of water. This could destroy the
195 pore structure of CLC mix, thereby reducing the stability of the foam. Oil/wax used for coating
196 the moulds will have no effect on the CLC mix, as the foam will already get embedded in the
197 mortar at that stage.

198

199 Test series with one control and seven different specimen series with different dosage of
200 macro and hybrid-synthetic polyolefin fibers (Figure 1) were prepared. Properties of macro and
201 micro fibers are given in Table 3. The plain concrete mix contains no fibers. FRCLC mix had
202 macro (ma) polypropylene fiber contents equal to 0.22%, 0.33%, 0.44% and 0.55%
203 respectively. Similarly, hybrid fiber (macro + micro(mi)) dosage consists of the following
204 combinations 0.22% ma + 0.02% mi; 0.33% ma +0.02% mi and 0.44% ma + 0.02% mi,

205 respectively. Three beam specimens of dimension 600 mm x 200 mm x 150 mm were cast for
206 each fiber dosage.
207

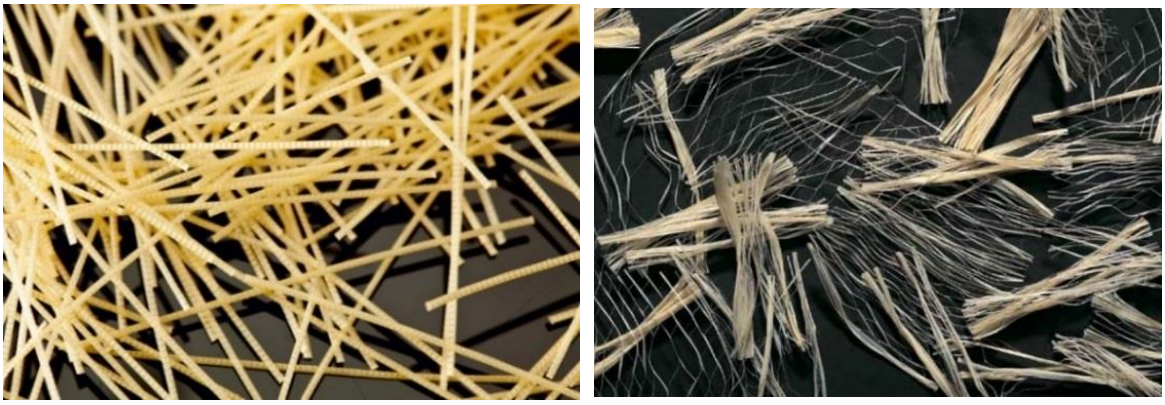

(a) Macro fiber (b) Micro fiber

208 Figure 1: Polyolefin fiber
209
210 Auxiliary specimens like cylinders of dimension 200 mm height and 100 mm diameter were
211 cast in addition during casting process and tested to determine the behavior under compression.
212 Similarly, dog-bone shaped specimens were tested under uni-axial tension. Summary of
213 compression and tension test results is given in Table 4. Compression toughness index (CTI)
214 and tension toughness index (TTI) values were calculated from the area under stress-strain
215 curves from the respective tests. Therefore, the unit of TTI and CTI will be those of energy per
216 unit volume that is N-mm per cubic millimeter which turns out to be MPa. Complete details of
217 uniaxial compression and tension tests and results can be found elsewhere [8], [10].
218
219 **TABLE 3.** Characteristics of the synthetic fibers

	Macro	Micro
Specification	Bi-component fiber	Inter-linked fiber
Length (mm)	50	19
Diameter (mm)	0.5	0.08
Density (g/cm^3)	0.91	0.91
Tensile Strength (N/mm^2)	618	400
Tensile Modulus (kN/mm^2)	10	4.9
Aspect ratio	100	237.5
Shape	Oval	Circle
Decomposition Temp (°C)	360	360

220

221 **TABLE 4.** Test Results of CLC under Compression and Tension with and without Fibers

Series	Specimen	Mean Compressive Strength (Standard Deviation) MPa	CTI (10^{-3}MPa)	Mean Tensile Strength (Standard Deviation) MPa	TTI (MPa)
I	Control	3.89(0.30)	6.99	0.13(0.37)	0.16
II (only macro)	ma-0.22-mi-0.00	5.94(0.92)	47.20	0.21(0.32)	30.2
	ma-0.33-mi-0.00	6.16(0.98)	54.90	0.32(0.73)	47.9
	ma-0.44-mi-0.00	6.58(0.52)	66.00	0.36(0.34)	58.1
	ma-0.55-mi-0.00	6.49(0.71)	63.50	0.44(0.18)	85.5
III (hybrid)	ma-0.11-mi-0.02	3.91(0.15)	57.55	-	-
	ma-0.22-mi-0.02	6.67(0.84)	68.27	0.28(0.14)	34.6
	ma-0.33-mi-0.02	8.39(0.90)	72.13	0.34(0.25)	52.5
	ma-0.44-mi-0.02	8.44(1.40)	78.46	0.41(0.25)	63.6

222 **Note:**

223 I. More details on compression and tension test results on CLC can be found in other paper of
224 authors [8], [10]
225 II. ma- macro fiber; mi- micro fiber; 0.11, 0.22, 0.33, 0.44, 0.55 – volume fraction of fibers in
226 %. CTI -Compressive toughness index, TTI- Tension toughness index.

227

228 **3.2. Test Setup**

229 Different codal provisions are available for determination of fracture energy of concrete
230 under flexure. RILEM committee report [38] has given recommendations for performing the
231 fracture test on notched concrete specimens under flexure. Based on these recommendations,
232 EN 14651:2005 [39] and JCI [40] standards has given test procedures for determination of
233 fracture parameters of concrete. For the purpose of this study, flexural testing was conducted
234 on notched beams as per the guidelines given in EN 14651:2005 [39]. CLC beams of size 600

× 200 × 150 mm were tested in the three-point bending configuration. A notch of 50 mm depth and 5 mm width was introduced at the mid-span using a circular saw as per the guidelines given in EN 14651 [39]. The flexure test was conducted in a crack mouth opening displacement control mode at a rate of 0.05 mm/min. A photograph of the test setup is shown in Figure 2.

3.3. Fracture Energy

Fracture energy (G_F) is the measure of energy absorbed by the specimen to undergo a unit area of crack formation through a predefined path. The area of crack is defined as the projected area on the plane parallel to main crack direction. The fracture energy of FRCLC were calculated using the guidelines provided in JCI-S-001-2003 [40]. The equations used for calculation of fracture energy are listed below.

$$G_F = \frac{0.75W_o + W_1}{A_{lig}} \qquad \text{Equation (1)}$$

$$W_1 = 0.75\left(\frac{S}{L}m_1 + 2m_2\right)g.CMOD_C \qquad \text{Equation (2)}$$

where G_F=Fracture Energy (N/mm^2); W_o= area below CMOD curve upto failure; W_1= work done by self-weight of specimen and loading jig; A_{lig}= Area of broken ligament; m_1= mass of specimen (kg); S= loading span (mm); L= total length of the specimen (mm); m_2= mass of jig not attached to testing machine but placed on machine until rupture (kg); g= gravitational acceleration (9.807m/s^2); $CMOD_C$=crack mouth opening displacement at failure (mm)

3.4. Acoustic Emission Monitoring

During the fracture test on notched specimens, four narrow band (50 kHz to 300 kHz) and four wide band (100 kHz to 1 MHz) AE sensors supplied by Physical Acoustics Corp. (PAC), USA were used. As far as the literature review done by authors is concerned, this study uses AE sensors to investigate the damage propagation in CLC for the first time. Therefore, two

types of sensors covering a wide spectrum of frequency is used in order to capture signals at large range of frequency. Analysis of AE data reveals that the average frequency of hits varied from 50kHz upto 350kHz. These sensors were attached to the beams at the locations defined by the coordinates given in Table 5. The test set-up along with the AE equipment is shown in the Figure 2. A close-up of AE sensors and amplifier is shown in Figure 3. In addition, a schematic of sensor placement is depicted in Figure 4. In this study, three dimensional event/source location of damage is attempted. The preamplifier gain was set to 40 dB. After performing a pilot test, the threshold was set to 40 dB in order to nullify the effect of electronic/environmental noise. Calibration of sensors was performed before each test to ensure proper bonding of the AE sensors to the surface. The signals were recorded in an eight-channel AE data acquisition (DAQ) card and the signals were recorded at a sampling rate of 5 MHz. For the purpose of calibration, lead pencil break test were performed on different locations on the surface of specimen. These calibration results showed the source location is within a range of 5% error. Therefore, the source location results remained less effected from the impedance difference between the foam, fibers and the concrete matrix.

TABLE 5. Co-ordinates of the AE sensors

Sensor number	X-co-ordinate (mm)	Y-coordinate (mm)	Z-coordinate (mm)
1.	175	0	50
2.	175	0	150
3.	275	0	50
4.	275	150	150
5.	175	150	50
6.	175	150	150
7.	275	150	50
8.	275	150	150

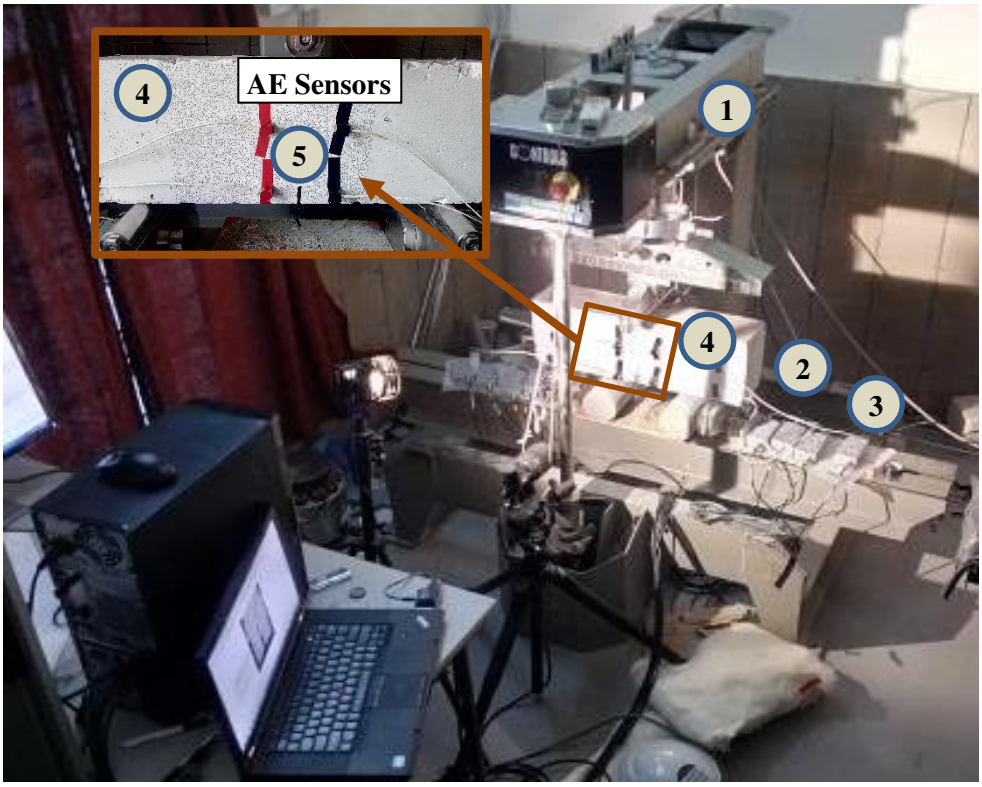

1. Controls Flexure Testing Machine 2. Notched FRCLC Specimen 3. Amplifier for AE Sensors 4. Positions of AE Sensors 5. Notch

Figure 2: Flexural Test Setup with Acoustic Emission Sensors

(a) Preamplifier (b) AE sensor

Figure 3: Close up view of Acoustic emission sensing components

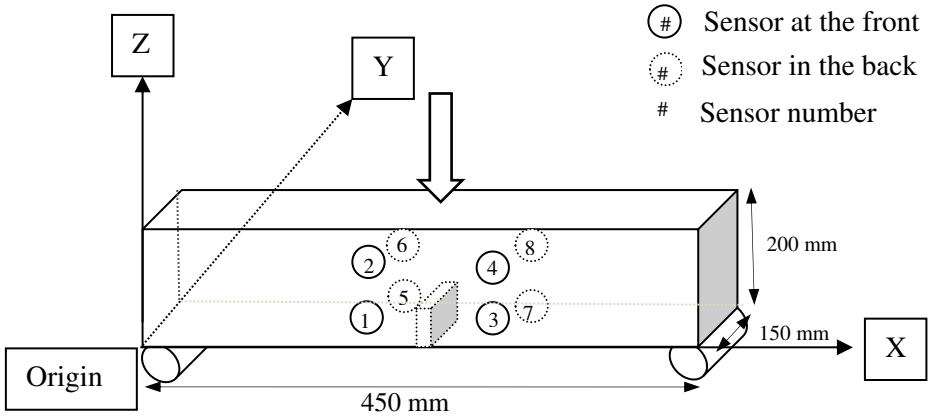

Figure 4: Schematic sketch for Acoustic Emission Sensor placement on notched FRCLC specimen

4. TEST RESULTS AND DISCUSSION

4.1. Flexural Fracture Test

The fracture properties state the structural contribution of the fibres in the load resistance of CLC. Residual strengths obtained from fracture tests are typically used in the structural design. The post-cracking properties are important to understand the efficiency of fibers in improving the ductility of CLC. Figure 5 shows the load versus crack mouth opening displacement response of notched FRCLC beams for different fibe dosages. Figure 5a and 5b shows the fracture behavior for CLC with macro and hybrid fibers, respectively. Upto the cracking of concrete matrix, the fiber reinforcement increases the cracking load of fiber reinforced CLC. After initiation of crack, the plain concrete exhibits decline in the load displacement response, whereas the fiber reinforced CLC performs better in terms of ductility and post-peak toughness. When macro fibers are elongated and pulled out from matrix, the energy would be consumed continuously in overcoming the interface strength between the fiber and the matrix resulting in significant improvement of the ductility of CLC. The post cracking load resistance is from fiber elongation followed by a combination of fiber pull-out and rupture. There is softening in the load response immediately after the peak load due to significant cracking and loss of stiffness.

In FRCLC specimens, there is an increase in the load carrying capacity with increasing crack opening (Figure 5a and 5b). The load recovery after the first cracking is initiated at a smaller value of crack opening displacement and a higher resistance is achieved during the load recovery with increase in the volume fraction of fibers. The increase in the residual load carrying capacity with increasing CMOD indicates that the macro synthetic fibers are efficient in providing crack closing stresses with increasing CMOD. The test results are summarized in Table 6. First cracking and peak loads increased with increasing fiber dosage. Moreover, the difference between cracking and peak load increased in beams with macro fiber dosage with increase in fiber dosage. However, the first cracking load increase in hybrid fiber reinforced

313 specimens and the difference between cracking and peak load reduced with increase in fiber
314 dosage.

315 Hybrid combination of macro and micro fiber as reinforcing components could increase
316 effectively the toughness and ability of CLC in resisting fracture. This is reflected in the load
317 vs CMOD curves (Figure 5c) that synergistic reinforcing effect between macro and micro fibers
318 were good. This is due to the fact that hybrid fibers with different lengths and diameter played
319 their corresponding roles at different scales. In micro-crack phase (CMOD < 0.1mm), micro
320 fiber can restrain crack development and restrict the propagation of micro-crack in matrix. In
321 macro-crack phase (CMOD > 0.1mm), micro fibers appeared to be less effective in controlling
322 the CLC matrix crack opening due to complete pull-out of micro fibers [41]. However, due to
323 relative larger interface strength between macro fiber and CLC matrix, the efficiency of macro
324 fibers in arresting the structural/macro cracks would be higher. When macro fibers are
325 elongated and pulled out from the CLC matrix, the energy would be consumed continuously,
326 and the ductility of CLC fiber reinforced composite improves significantly. When the total
327 fiber volume fractions are kept the same, the reinforcement effects of hybrid combination of
328 macro and micro fibers is much better than the CLC specimens with only macro fibers. For
329 example, the addition of 0.02% of micro fibers with 0.4% macro fiber resulted in improvement
330 of 34% in fracture load. However, no difference in peak load was observed between hybrid and
331 macro fiber reinforced CLC (Table 6, Figure 5c).
332

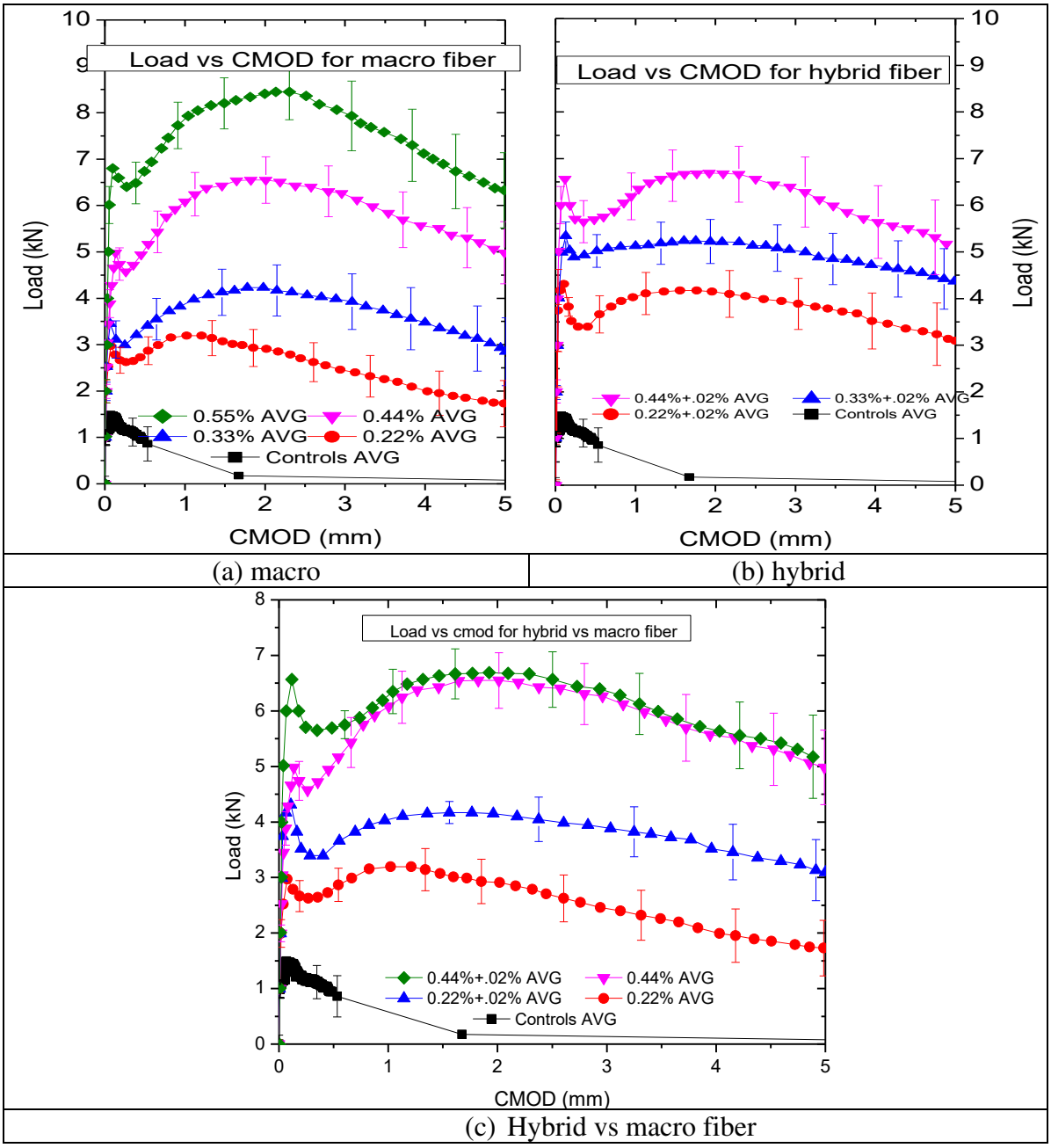

Figure 5: Load vs Avg. CMOD opening of FRCLC under flexure

4.2. Cracking Modes

Change in crack patterns with increase in fiber dosage at failure indicates the change in failure mode. Figure 6 shows the visual crack opening modes of the tested specimens. Figure 6(a) and 6(b) shows the front and back view of visual crack opening modes in plain CLC. Control specimen showed a brittle response in flexure, wherein the crack path was observed to be perpendicular to the bending axis of the specimen. This may be a result of very little resistance offered by matrix in post-crack formation stage. On the other hand, crack growth in

FRCLC specimen was observed to be meandering along the plane of notch. This can be attributed to the low strength of the matrix and high strength of fiber, which makes the crack path to search for the path of least resistance inside the matrix where fibers are randomly distributed (Figure 6c).

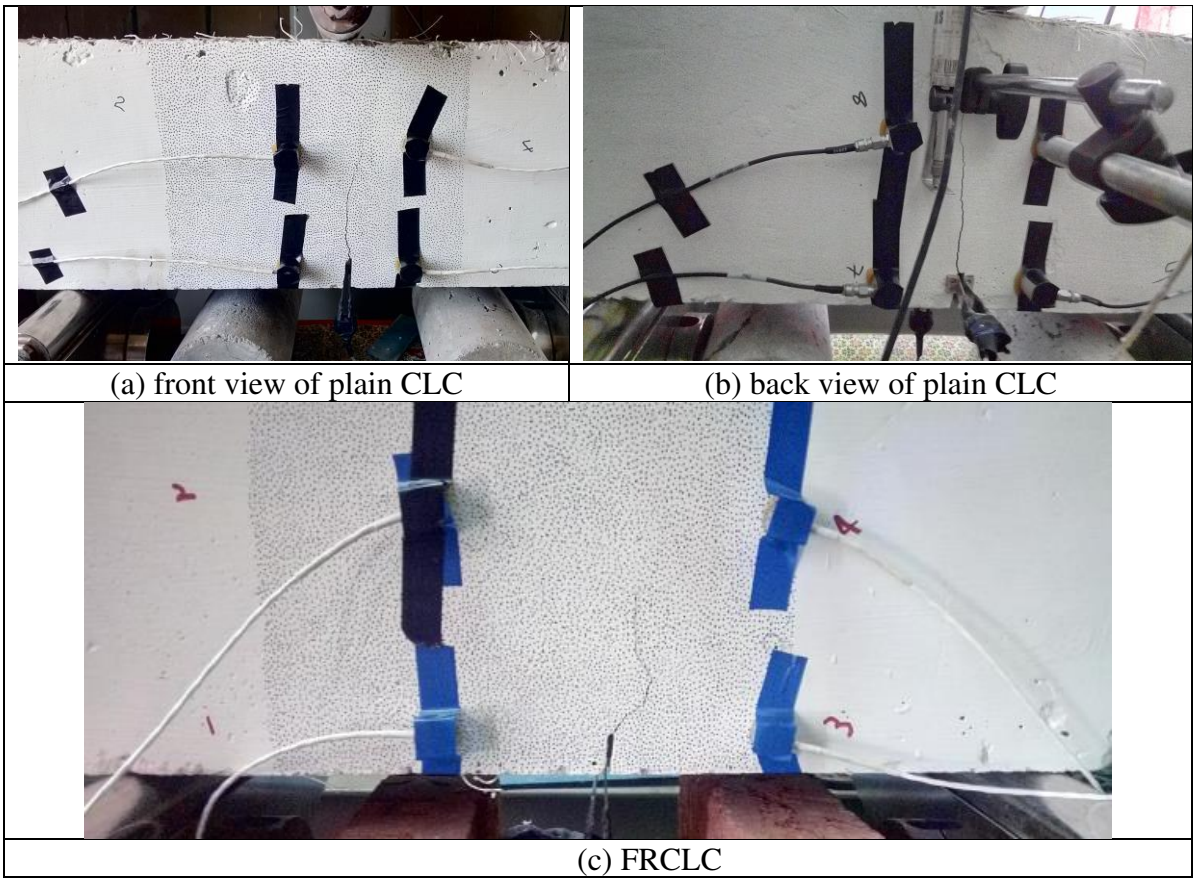

(a) front view of plain CLC (b) back view of plain CLC

(c) FRCLC

Figure 6: Cracking of CLC under flexure

4.3. Acoustic hits and Energy Dissipation

In order to clarify the fracture resistance, acoustic emission (AE) monitoring is employed during fracture tests. Acoustic energy emission is the phenomenon where the strain energy stored inside the specimen gets transmitted through the material, when it is subjected to stress generated by load application or thermal gradient. This energy is transmitted in the form of elastic waves and gets picked up by AE sensors. The first part of AE analysis deals with the plotting of cumulative AE energy and AE counts with respect to load vs CMOD. This results

355 in a quantitative estimate of crack opening and load when a certain value of AE energy and
356 counts are obtained. Failure in CLC can be due to matrix cracking and interface failure between
357 the voids and CLC matrix. The possibility of delaying the crack growth due to fibre action
358 increases with increasing fibre volume content. Consequently, the material toughness is
359 enhanced. In fiber reinforced CLC, the fibre pull-out also contributes to the final failure. The
360 distinct fracture mechanisms emit AE signals with different characteristics. Therefore, many
361 AE parameters of the recorded waves such as rise time, count, amplitude and duration are
362 studied in order to understand the distinct failure mechanisms in CLC.
363
364 The number of counts in a particular hit gives the idea of relative difference within the
365 domain of hits. The authors have observed a smooth trend when cumulative number of counts
366 were plotted against the CMOD. The plot of AE energy vs CMOD showed a couple of hikes
367 in the curve due to the fiber breaking instances. Hence to ascertain the crack width at a
368 particular instant of AE counts number of counts are considered in a cumulative approach.AE
369 activity is very important as high rate of AE recording is linked to high rate of crack
370 propagation. Similarly, very little or limited AE activity implies lesser crack propagation. Thus,
371 the total number of AE hits recorded with respect to the measurement time is the fundamental
372 parameter for understanding the role of fibers in crack arresting. Figure 7a & 8a shows the
373 variation of cumulative acoustic energy against the applied load with respect to increasing
374 value of CMOD for macro fibers and hybrid fibers, respectively. For both cases, three different
375 fiber dosages such as 0.33%, 0.44% and 0.55% are considered for evaluation. Hybrid fiber
376 dosage included a constant dosage of 0.02% micro fibers in addition to macro fibers.
377
378 The recorded energy at both sensors is combined for the calculation of cumulative energy.
379 The combined energy is a superposition of the energy received from both types of sensors. The

trend of energy recorded vs CMOD remains the same even if only one type of sensors are used. However, the numbers may vary accordingly. Energy and counts are plotted using data from all the sensors rather than just the source location data. The source location points are generated for hits where at least three sensor data coincides at a point. This may not be recorded for all the hits generated. Energy and counts from the source location data alone are lesser compared to the overall data captured which can under predict the actual AE energy and the generated counts. Therefore, all the data recorded by the eight sensors are used to investigate the AE energy and the cumulative number of counts. Cumulative AE counts with load vs CMOD are compared in Figure 7b and 8b for macro and hybrid fibers, respectively. Number of AE events increased significantly up to the peak load and the rate of increase in AE events reduced after peak load in both the beams with macro and hybrid fibers. Before cracking, lesser number of AE hits and AE energy was recorded. After the load drop, the increase in AE rate decreases but it does not cease completely. Concerning the mechanical behavior, soon-after the first macro-crack develops, load typically drops by several kN. The AE energy is found to increase with increase in fiber dosage (Figure 7a & 8a). Using this information, the damage behavior of structural element can be quantified for the average crack opening recorded between the AE sensor configuration.

Figure 9a and 9b shows the plot of CMOD against the number of cumulative AE counts for macro and hybrid fibers, respectively. The increase in number of AE hits and AE energy in the post-cracking region can be attributed to the fiber pull-out and breaking of fibers. Normalized AE energy vs fracture energy of FRCLC under flexure is plotted in Figure 10. It clearly shows that the addition of synthetic fibers significantly improved the fracture behavior of CLC. Addition of even a small amount of micro fibers in hybrid fiber combination significantly increased the fracture energy of CLC when compared to only macro fiber addition. For

405 example, the fracture energy (GF) of CLC with 0.44% volume fraction of macro fibers
406 increased by a factor of three when compared to control beam.
407

	Macro fiber 0.33%	Macro fiber 0.44%	Macro fiber 0.55%
(a) Load vs CMOD vs Cum. Energy	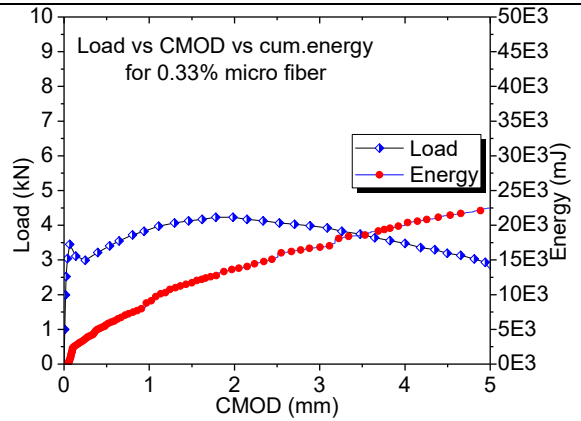	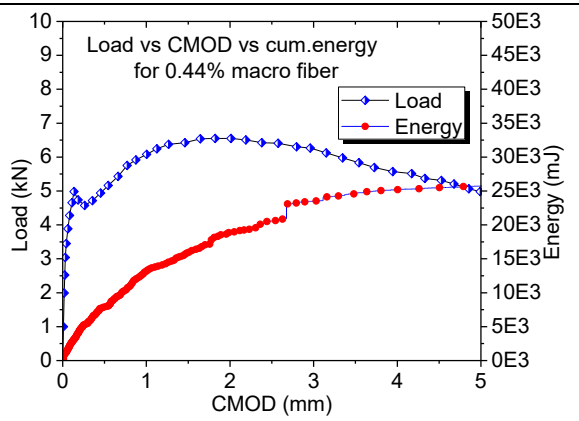	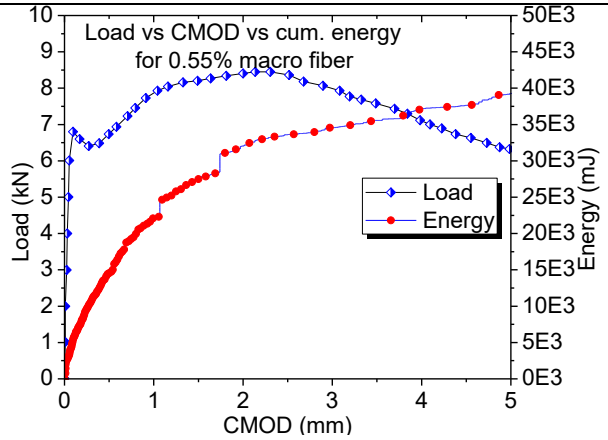
(b) Load vs CMOD vs Cum. Counts	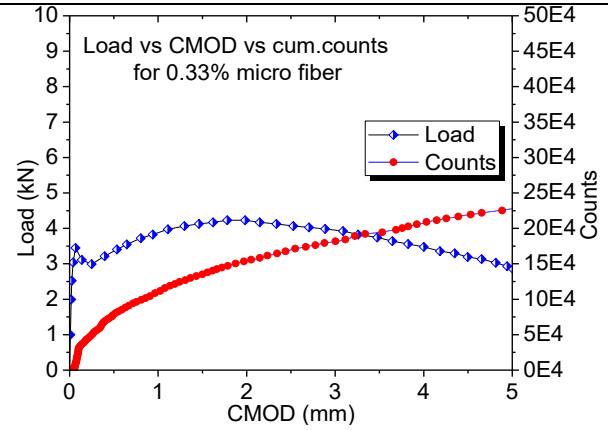	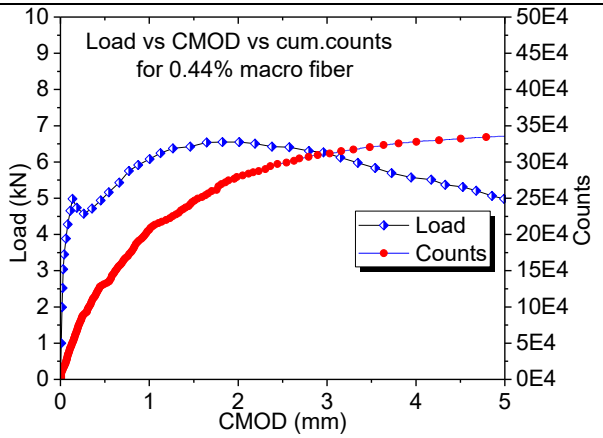	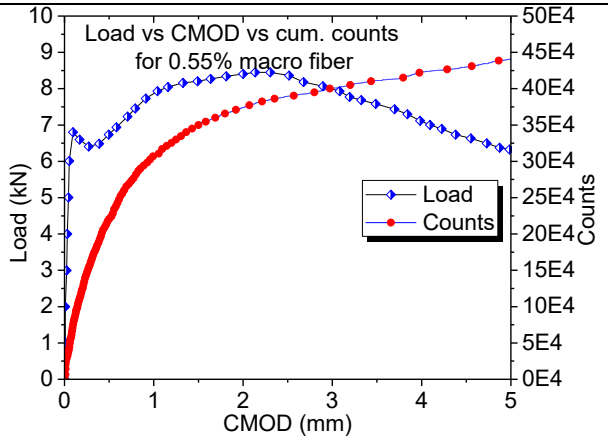

Figure 7: Load vs CMOD vs Energy/Cum. Counts for Macro FRCLC under Flexure

	Hybid fiber 0.22%+0.02%	Hybrid fiber 0.33%+0.02%	Hybrid fiber 0.44%+0.02%
(a) Load vs CMOD vs Cum. Energy	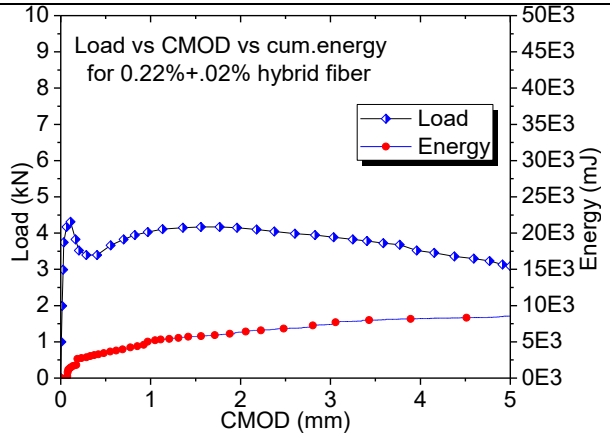	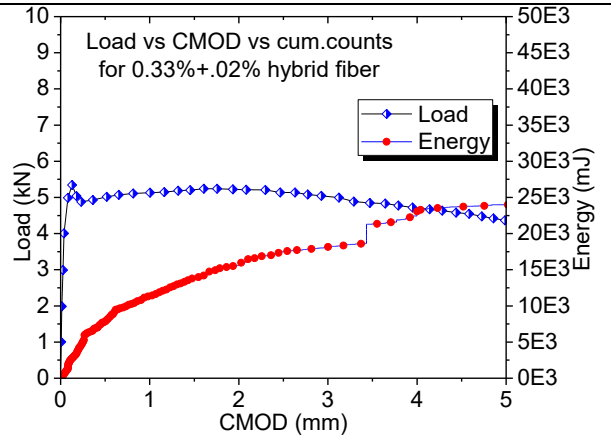	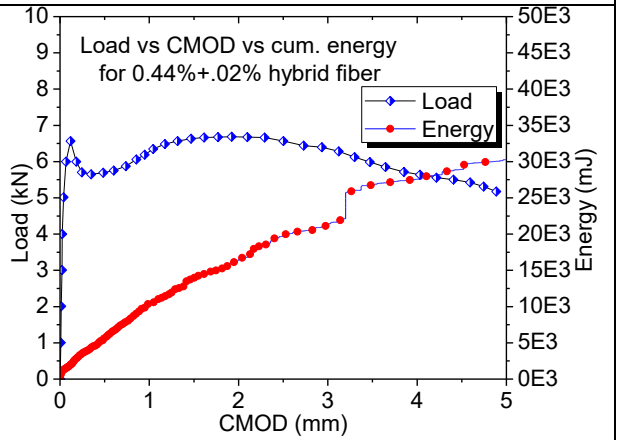
(b) Load vs CMOD vs Cum. Counts	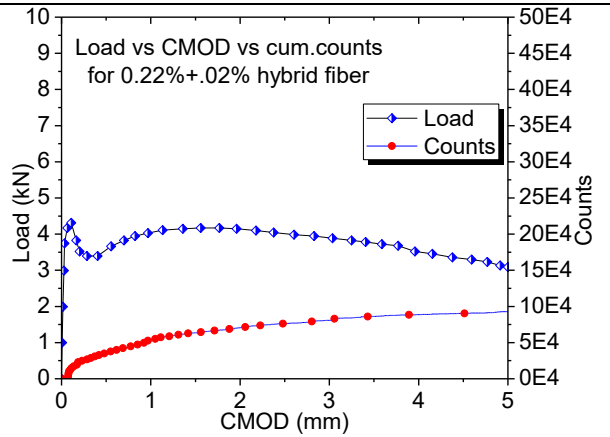	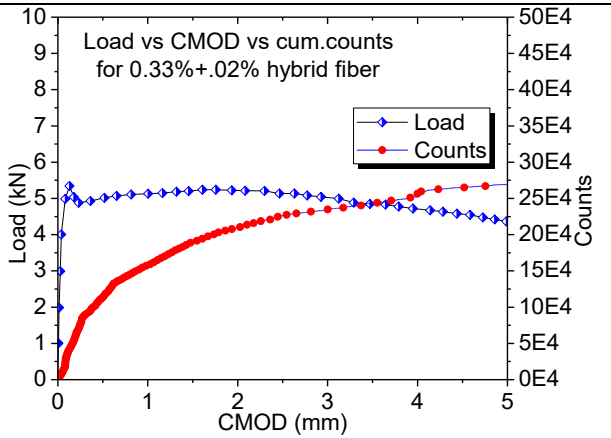	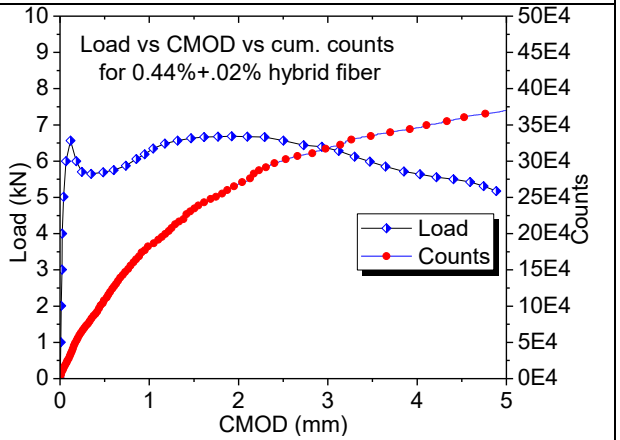

Figure 8: Load vs CMOD vs Energy/Cum. Counts for hybrid FRCLC under flexure

409

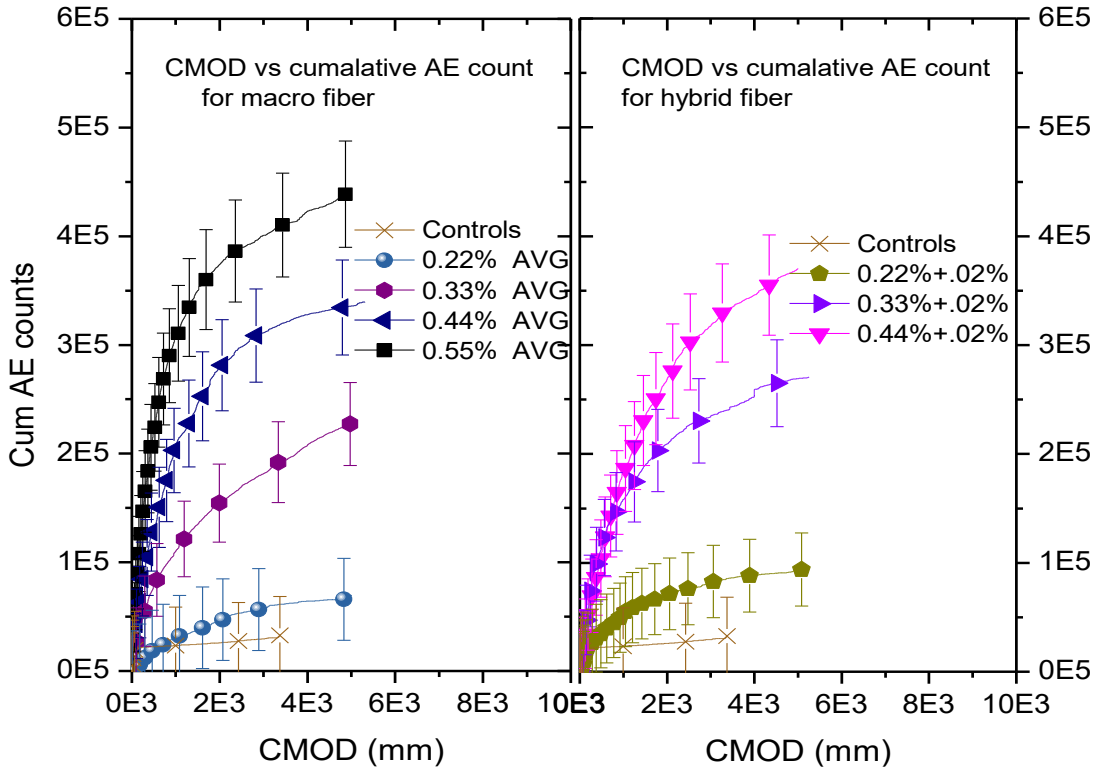

Figure 9: Cumulative AE count vs Avg. CMOD opening of FRCLC under flexure

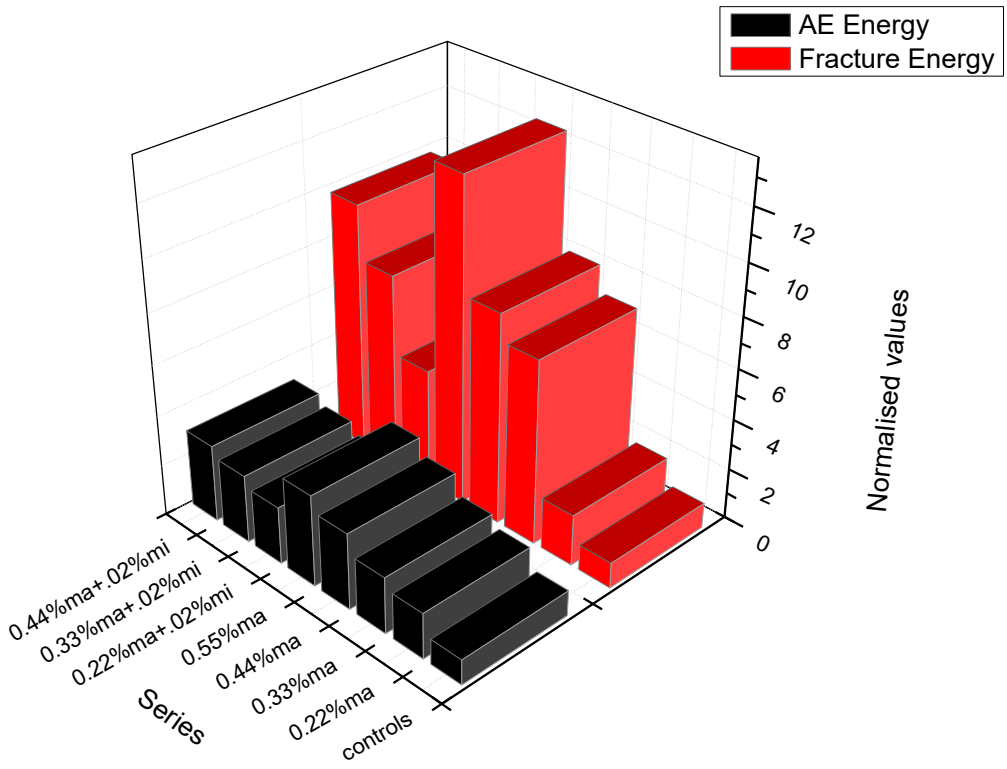

414

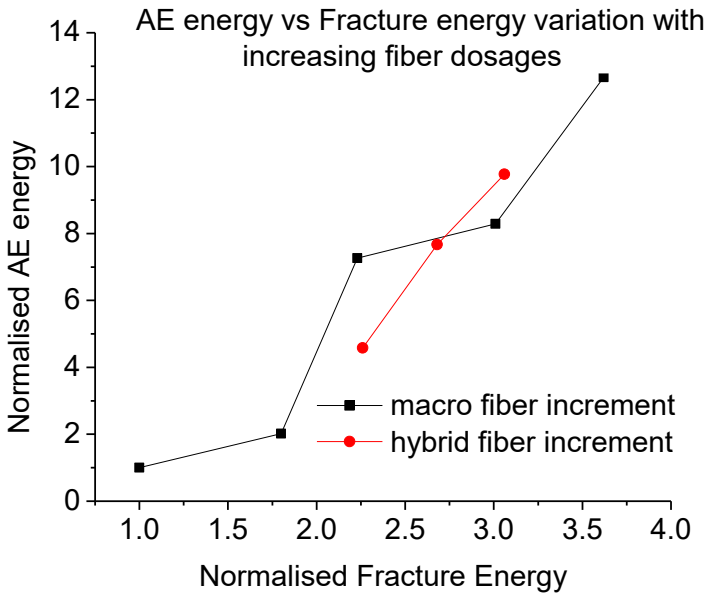

415

416 Figure 10: Normalized AE energy vs fracture energy of FRCLC under flexure
417

418 **5. IDENTIFICATION OF 3D-CRACK LOCATION AND DIFFERENTIATION OF**
419 **CRACKING MODE**

420 Identification of fracture process zone (FPZ) is of prime importance in structural health

421 monitoring and retrofitting of structural elements. AE source location can be potentially applied

422 to identify FPZ. Furthermore, the mode of failure has to be properly distinguished in order to
423 understand the global failure mechanism in a structural element. The dimension of specimen
424 i.e, 450 mm length 150 mm width and 200 mm height during the test were simulated for 3D
425 crack location and differentiation of cracking modes using a MATLAB program. The second
426 part of AE analysis deals with the detection of source location. Every sensor generates a
427 distance from which it is picking up a particular signal, which may be visualized in the form
428 of a hollow sphere. At the same time, if two or more signals are picking up the same signal, the
429 overlap of these three signals results in the hit source location which can be visualized as
430 intersection point between three hollow spheres. For the located signal, the corresponding RA
431 value and Average Frequency values are calculated and their ratio is used to differentiate the
432 localized mode of failure. The initiation of AE event and its mode of failure at a local level
433 may correspond to matrix cracking or fiber pull-out, which then can be correlated to mode I or
434 mode II, respectively. The differentiation of different AE events was done based on the
435 parameter based method. Definitions of different terms used in AE analysis is defined in Figure
436 11a. RA value is defined as the ratio of the rise time to the waveform amplitude. Average
437 frequency is defined as the number of threshold crossings (counts) divided by the duration of
438 the signal (Figure 11a). It is expressed in kHz. Analysis of AE results based on parameter
439 based method (Figure 11b) helps to differentiate the tensile and shear mode. The parameter
440 based method involves calculation of two parameters viz,. RA value and Average Frequency
441 (AE ring-down counts/Duration time) and plotting them on X and Y axis respectively as shown
442 in Figure 11a. The events are then classified based on the region which they lie as shown in the
443 Figure 11b.

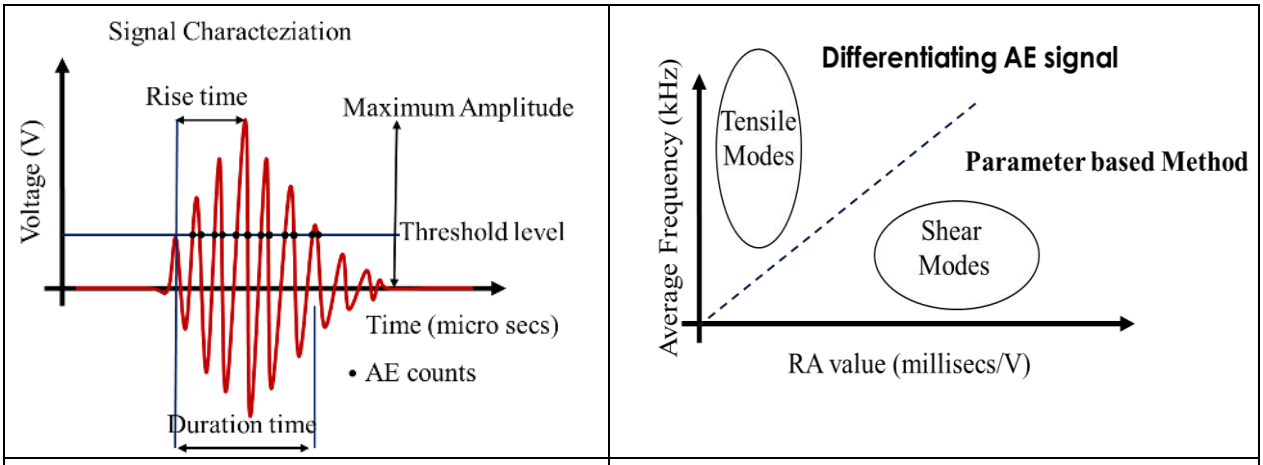

(a) Definitions of Terms in AE | (b) Two Different Modes from AE Parameter

Figure 11: Differentiation of AE events from FRCLC under flexure

In general, the tensile cracks in mode I produces AE signals with high frequency. However, the shear type of crack (mode II) produces AE signals of lower frequency. Initially, tensile matrix cracking (mode 1) initiated on the tension side (bottom surface) due to tensile stresses. At higher loads, with extension of crack to the compression side, occurrence of fiber friction and pull-out events (shear, mode II) begins. In the final stages close to failure, the fibre pull-out events dominate the process when the two parts of the CLC specimen separates completely. Previous studies on crack classification in concrete based on AE has shown that the value of slope of line, which differentiates the modes of failure, can be kept as 200 for a good correlation with SiGMa procedure. For the purpose of this study of FRCLC, the slope value of 200 gives a good correlation with SiGMa procedure [9,10,14].

Normalized values of AE and fracture energy shows a trend with AE energy values close to almost three times that of fracture energy values for higher fiber dosages. Summary of results including cracking load, peak load, fracture energy and AE energy are summarized in Table 6. This shows that the measurement of AE energy has a direct correlation with the fracture energy and toughness of the CLC. Moreover, addition of fibers increases the cumulative AE energy.

AE energy for hybrid fiber reinforced CLC was higher than that of CLC beams with only macro fibers. Figure 12 shows the AE crack source location in three dimensional space for fiber reinforced CLC for different fiber dosages. Figure 12a shows the schematic of specimen which is taken as a reference in subsequent figures for source location. Figure 12b shows the crack source location for controls specimen. It is clearly observed that the dominant event in AE source location is mode I. Figure 12c and 12d shows the crack source location for macro fiber reinforced CLC with 0.55% and 0.44% respectively. Similarly, the Figure 12e and 12f show the crack source location for hybrid fiber reinforced CLC with 0.33% and 0.44% of macro fiber dosage with a constant micro fiber dosage of 0.02%. The corresponding distribution of events and their failure modes were plotted on histograms along the length and height of the specimen and placed on the top and right side, respectively. The events that were recorded during the testing were differentiated as two modes of failure viz., shear and tensile mode. Plain CLC failure failed in tensile mode of failure. FRCLC showed a predominant shear mode of failure at high fiber dosages (Figure 12). Failure of FRCLC can be observed from the histograms of number of events corresponding to shear and tensile modes that are plotted alongside the AE hits. It can also be identified from the histograms that there is a normal distribution trend of AE events followed along the length of the specimen. The relative ratio of contribution from shear modes is shown to increase along the length as well as along the height directions. The tensile modes increase towards the downward region of the notch, whereas the shear modes increase from top, reaches a maximum value and then decreases towards the downward region. It is also observed that the fiber reinforcement tends to shift the mode of failure from tensile to shear mode.

The results of this analysis shows that the amount of AE activity is proportional to the fiber dosage and fracture toughness. Parameter based analysis of AE data shows that the tensile

mode of fracture is dominant for plain CLC. The mode of fracture is changing to shear with increase in fiber dosage. This demonstrates the reinforcing effect of the fibres against the weak tensile behavior of CLC. The study of AE indices implies that the mode of fracture changes during the experiment from tensile (initial stage) to shear (final fracture). This is macroscopically shown by the crack splitting and deflection from parallel to perpendicular direction relatively to the loading axis. In addition, the fracture process zone increases simultaneously with increasing fiber content. Though limited specimens were tested, the results are promising and provide confidence that acoustic emission technique can be used for the identification of the different fracture modes. Source location and identification of cracking behavior provides valuable insight for choosing optimum fiber dosage at a given stress state. Moreover, crack classification using suitable AE descriptors shown in in Figure 11b can assist in the evaluation of the severity of the condition as the shear mode typically follows the tensile mode in fiber reinforced CLC.

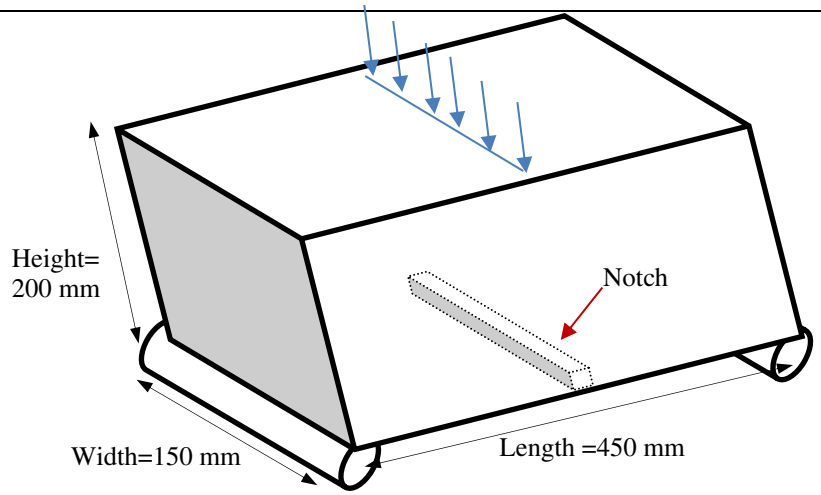

(a) Schematic of specimen

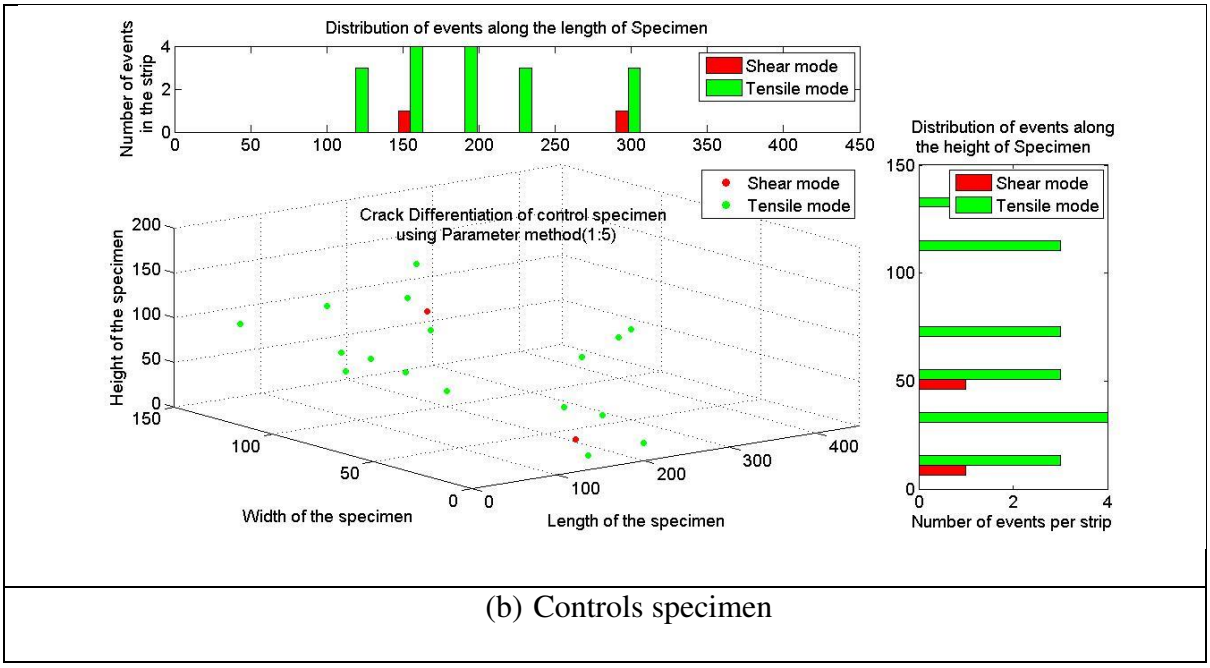

(b) Controls specimen

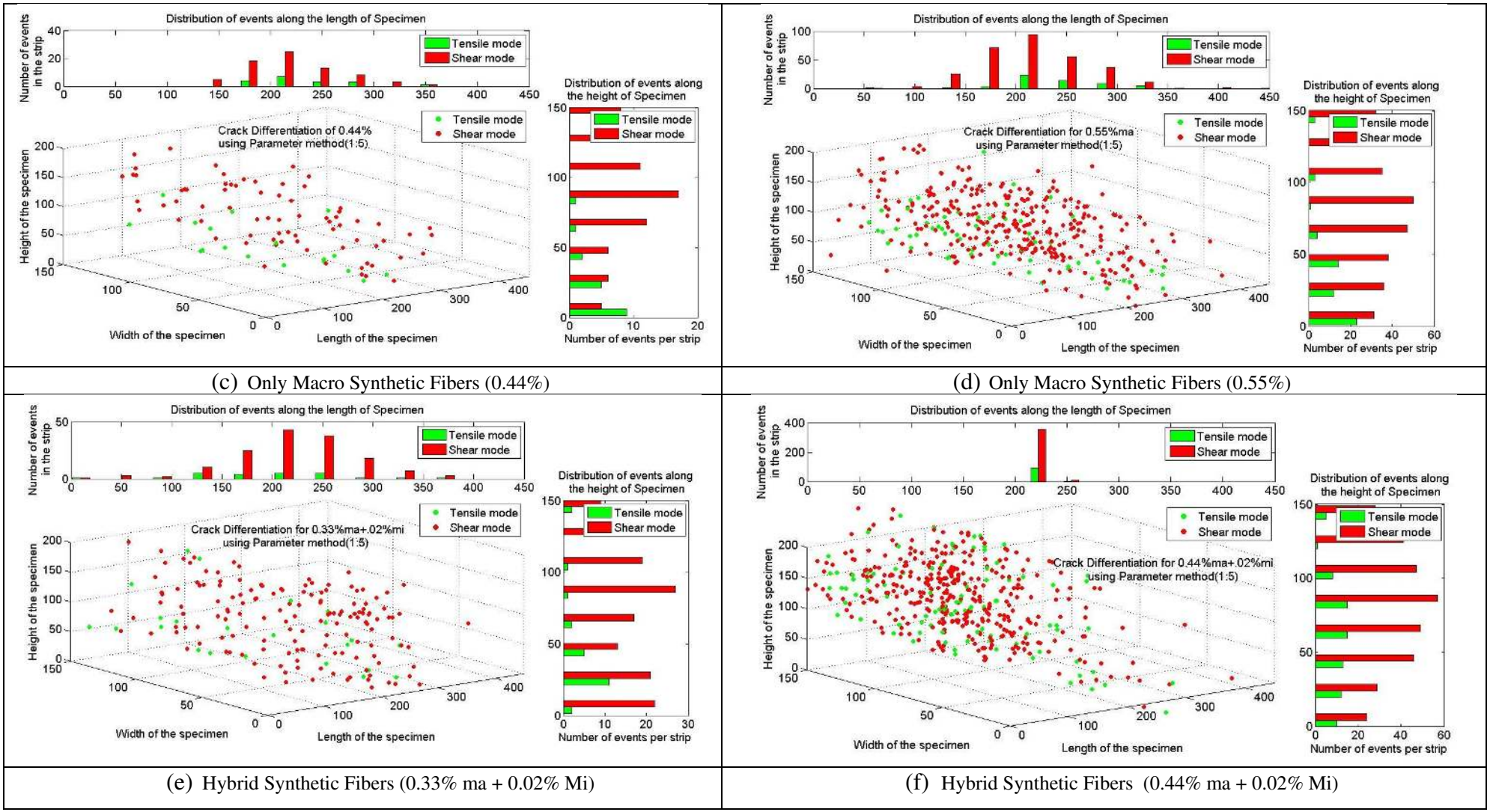

(c) Only Macro Synthetic Fibers (0.44%)

(d) Only Macro Synthetic Fibers (0.55%)

(e) Hybrid Synthetic Fibers (0.33% ma + 0.02% Mi)

(f) Hybrid Synthetic Fibers (0.44% ma + 0.02% Mi)

Figure 12: AE hit source location of FRCLC using AE sensors under flexure

TABLE 6. Fracture parameters and AE energy values.

Series	Specimen	Peak Load (kN)			Mean Peak Load (kN)	Standard Deviation (kN)	Fracture Load (kN)	W_o (N/mm^2)	G_F (N/mm^2)	Normalized G_F	Acoustic Emission Energy (J)	Normalized Acoustic Emission Energy
		1	2	3								
I	Control	1.75	1.22	1.48	1.49	0.37	1.49	1.71	605.7	1.00	3.1	1.00
II (only Macro)	ma-0.2-mi-0.0	3.26	3.46	2.83	3.19	0.32	2.96	12.65	1091.9	1.80	7.9	2.02
	ma-0.3-mi-0.0	3.48	4.26	4.94	4.23	0.73	3.44	18.49	1351.5	2.23	22.5	7.26
	ma-0.4-mi-0.0	5.88	6.79	6.96	6.55	0.58	4.98	28.99	1818.2	3.01	25.7	8.29
	ma-0.5-mi-0.0	9.35	8.20	7.79	8.45	0.81	6.80	37.40	2191.9	3.62	39.3	12.67
III (hybrid)	ma-0.2-mi-0.02	4.98	3.92	4.02	4.31	0.59	4.31	18.92	1370.7	2.26	14.2	4.58
	ma-0.3-mi-0.02	5.01	4.89	6.11	5.34	0.67	5.34	24.61	1623.5	2.68	23.8	7.67
	ma-0.4-mi-0.02	7.01	5.69	6.97	6.56	0.75	6.69	29.73	1851.1	3.06	30.3	9.77

Note:

- ma- macro fiber; mi- micro fiber; 0.2, 0.3, 0.4, 0.5 – volume fraction of fibers in %.
- G_F - Fracture Energy (N/mm^2); W_0 - area below CMOD curve up to rupture of specimen

6. SUMMARY AND CONCLUSIONS

Notched fiber reinforced CLC beams were tested under flexure to understand the fracture and acoustic emission behavior. Fracture tests for FRCLC has been performed and variation of CMOD with respect to different fiber dosages was studied. Various AE parameters such as energy and cumulative counts were plotted against the applied load and CMOD. Cumulative AE count is established against the CMOD in an attempt to quantify the crack opening using the AE technique. In addition to this, 3D source location of cracks and cracking modes was carried out. Based on the limited results presented in this study, the following major conclusions can be drawn:

- Addition of synthetic fibers significantly improves the fracture behavior of CLC. Addition of even a small amount of micro fibers in hybrid fibers, significantly improves the toughness and ductility of CLC when compared to only macro fiber addition. For instance, the fracture energy of CLC beams with 0.44% volume fraction of macro fibers increased by a factor of three when compared to control CLC beams.
- Acoustic emission energy increases with increase in fiber dosage. This directly correlates to the increase in strain energy absorbed during the fracture process.
- Crack width can be measured indirectly through the number of AE hits observed. CMOD measurement correlated with the number of AE hits.
- 3D source analysis gave a consistent result when compared to the actual crack growth observed in the test results. With increase in fiber dosage, a clear shift of failure from tensile to shear mode was observed.

Density is a very important parameter that affects the mechanical properties of CLC. Future work should focus on understanding the AE monitoring of CLC elements by including

various parameters such as different types and volume fractions of fibers and the effect of density on the fracture behavior of fiber reinforced CLC.

ACKNOWLEDGEMENTS

This work has been carried out as a joint collaboration between Indian Institute of Technology Hyderabad, India and Ritsumeikan University, Japan. The authors gratefully acknowledge the financial support lend by Department of Science and Technology, India through Grant No: SR/S2/RJN-30/2012, YSS/2015/000677. Brugg Contec AG and Grenix Infrastructure Ltd donated the fibers for this research. The authors duly acknowledge their support.

REFERENCES

[1] B. Zhang and C. S. Poon, "Use of Furnace Bottom Ash for producing lightweight aggregate concrete with thermal insulation properties," *J. Clean. Prod.*, vol. 99, pp. 94–100, 2015.

[2] K. Ramamurthy, E. K. K. Nambiar, and G. I. S. Ranjani, "Cement & Concrete Composites A classification of studies on properties of foam concrete," *Cem. Concr. Compos.*, vol. 31, no. 6, pp. 388–396, 2009.

[3] M. R. Jones and A. Mccarthy, "Preliminary views on the potential of foamed concrete as a structural material," no. 1, pp. 21–31, 2005.

[4] Z. Zhang, J. L. Provis, A. Reid, and H. Wang, "Geopolymer foam concrete: An emerging material for sustainable construction," *Constr. Build. Mater.*, vol. 56, pp. 113–127, 2014.

[5] R. F. Zollo and C. D. Hays, "Engineering material properties of a fiber reinforced cellular concrete," *ACI Mater. J.*, vol. 95, no. 5, pp. 631–635, 1998.

[6] M. A. Rasheed and S. S. Prakash, "Effect of Synthetic Fiber Reinforcement on Compression and Tension Behavior of Cellular Lightweight Concrete," in *9th RILEM International Symposium on Fiber Reinforced Concrete- BEFIB 2016, Vancouver, Canada*, no. 9, pp. 632–641.

[7] M. A. Rasheed and S. S. Prakash, "Experimental study on compression behavior of fiber reinforced cellular concrete stack bonded masonry prisms," *ACI Mater. J.*, 2018.

[8] M. A. Rasheed and S. S. Prakash, "Mechanical behavior of sustainable hybrid-synthetic fiber reinforced cellular light weight concrete for structural applications of masonry," *Constr. Build. Mater.*, vol. 98, pp. 631–640, 2015.

[9] S. Jain, S. S. Prakash, and K. V. L. Subramaniam, "Monitoring of Concrete Cylinders With and Without Steel Fibers Under Compression Using Piezo-Ceramic Smart Aggregates," *J. Nondestruct. Eval.*, pp. 1–7, 2016.

[10] M. A. Rasheed and S. S. Prakash, "Behavior of Hybrid-Synthetic Fiber Reinforced

Cellular Lightweight Concrete under Uni-axial Tension - Experimental and Analytical Studies," *Constr. Build. Mater.*, no. 29 (Accepted), 2017.

[11] M. A. Rasheed and S. S. Prakash, "Flexural Behavior of Synthetic Fiber Reinforced Cellular Light Weight Concrete," in *2nd R.N.Raikar International Conference and Banthia-Basheer International Symposium on Advances in Science and Technology of Concrete, Mumbai, India*, 2015, pp. 1–7.

[12] M. A. Rasheed and S. S. Prakash, "Compression Behavior of Synthetic Fiber Reinforced Cellular Concrete Masonry Prisms," in *2nd R.N.Raikar International Conference and Banthia-Basheer International Symposium on Advances in Science and Technology of Concrete, Mumbai, India*, 2015, no. 2, pp. 1–5.

[13] J. Huang, Q. Su, W. Zhao, T. Li, and X. Zhang, "Experimental study on use of lightweight foam concrete as subgrade bed filler of ballastless track," *Constr. Build. Mater.*, vol. 149, pp. 911–920, 2017.

[14] M. Koz, M. Kadela, and A. Kukie, "Fracture energy of foamed concrete based on three-point bending test on notched beams," *Procedia Eng.*, vol. 108, pp. 349–354, 2015.

[15] B. Trunk, G. Schober, A. K. Helbling, and F. H. Wittmann, "Fracture mechanics parameters of autoclaved aerated concrete," *Cem. Concr. Res.*, vol. 29, pp. 855–859, 1999.

[16] K. Ohno, K. Uji, A. Ueno, and M. Ohtsu, "Fracture process zone in notched concrete beam under three-point bending by acoustic emission," *Constr. Build. Mater.*, 2014.

[17] M. Ohtsu and H. Watanabe, "Quantitative damage estimation of concrete by acoustic emission," *Constr. Build. Mater.*, vol. 15, pp. 217–224, 2001.

[18] J. Berthelot, M. Ben Souda, and J. L. Robert, "Identification of Signals in the Context of Acoustic Emission in Concrete," *J. Nondestruct. Eval.*, vol. 13, no. 2, pp. 63–73, 1994.

[19] M. G. R. Sause and S. Richler, "Finite Element Modelling of Cracks as Acoustic Emission Sources," *J. Nondestruct. Eval.*, vol. 34, no. 4, pp. 1–13, 2015.

[20] E. N. Landis and S. P. Shah, "Recovery of Microcrack Parameters in Mortar Using Quantitative Acoustic Emission," *J. Nondestruct. Eval.*, vol. 12, no. 4, pp. 219–232, 1993.

[21] D. Soulioti, N. M. Barkoula, A. Paipetis, T. E. Matikas, T. Shiotani, and D. G. Aggelis, "Acoustic emission behavior of steel fibre reinforced concrete under bending," *Constr. Build. Mater.*, vol. 23, no. 12, pp. 3532–3536, 2009.

[22] N. Nor, A. Ibrahim, N. Muhamad, and H. Mohd, "Acoustic emission signal for fatigue crack classification on reinforced concrete beam," *Constr. Build. Mater.*, vol. 49, pp. 583–590, 2013.

[23] S. Hu, J. Lu, and F. Xiao, "Evaluation of concrete fracture procedure based on acoustic emission parameters," *Constr. Build. Mater.*, vol. 47, pp. 1249–1256, 2013.

[24] Y. Kawasaki, T. Kobarai, and M. Ohtsu, "Kinematics of Corrosion Damage Monitored by Acoustic Emission Techniques and Based on a Phenomenological Model Kinematics of Corrosion Damage Monitored by Acoustic Emission Techniques and Based on a Phenomenological Model," *J. Adv. Concr. Technol.*, vol. 10, pp. 160–169, 2012.

[25] Y. Kawasaki, S. Wasada, T. Okamoto, and K. Izuno, "Evaluation for RC specimen damaged from rebar corrosion by acoustic emission technique," *Constr. Build. Mater.*, vol. 67, pp. 1–8, 2014.

[26] A. Zaki, H. Kian, A. Behnia, D. G. Aggelis, J. Ying, and Z. Ibrahim, "Monitoring fracture of steel corroded reinforced concrete members under flexure by acoustic

emission technique," *Constr. Build. Mater.*, vol. 136, pp. 609–618, 2016.

[27] H. A. Elfergani, R. Pullin, and K. M. Holford, "Damage assessment of corrosion in prestressed concrete by acoustic emission," *Constr. Build. Mater.*, vol. 40, pp. 925–933, 2013.

[28] A. K. M. F. Uddin, K. Numata, J. Shimasaki, M. Shigeishi, and M. Ohtsu, "Mechanisms of crack propagation due to corrosion of reinforcement in concrete by AE-SiGMA and BEM," *Constr. Build. Mater.*, vol. 18, pp. 181–188, 2004.

[29] A. A. Abouhussien and A. A. A. Hassan, "The Use of Acoustic Emission Intensity Analysis for the Assessment of Cover Crack Growth in Corroded Concrete Structures," *J. Nondestruct. Eval.*, vol. 35, no. 3, pp. 1–14, 2016.

[30] Y. Kawasaki, T. Wakuda, T. Kobarai, and M. Ohtsu, "Corrosion mechanisms in reinforced concrete by acoustic emission," *Constr. Build. Mater.*, vol. 48, pp. 1240–1247, 2013.

[31] D. G. Aggelis, A. C. Mpalaskas, and T. E. Matikas, "Investigation of different fracture modes in cement-based materials by acoustic emission," *Cem. Concr. Res.*, vol. 48, pp. 1–8, 2013.

[32] M. A. A. Aldahdooh and N. M. Bunnori, "Crack classification in reinforced concrete beams with varying thicknesses by mean of acoustic emission signal features," *Constr. Build. Mater.*, vol. 45, pp. 282–288, 2013.

[33] D. G. Aggelis, S. Verbruggen, E. Tsangouri, T. Tysmans, and D. Van Hemelrijck, "Characterization of mechanical performance of concrete beams with external reinforcement by acoustic emission and digital image correlation," *Constr. Build. Mater.*, vol. 47, pp. 1037–1045, 2013.

[34] S. Rouchier, G. Foray, N. Godin, M. Woloszyn, and J. Roux, "Damage monitoring in fibre reinforced mortar by combined digital image correlation and acoustic emission," *Constr. Build. Mater.*, vol. 38, pp. 371–380, 2013.

[35] S. Verbruggen, S. De Sutter, S. Illipoulos, T. Tysmans, and D. G. Aggelis, "Experimental Structural Analysis of Hybrid Composite-Concrete Beams by Digital Image Correlation (DIC) and Acoustic Emission (AE)," *J. Nondestruct. Eval.*, vol. 35, no. 2, pp. 1–10, 2016.

[36] K. Ohno and M. Ohtsu, "Crack classification in concrete based on acoustic emission," *Constr. Build. Mater.*, vol. 24, no. 12, pp. 2339–2346, 2010.

[37] IS 2185-4, "Concrete masonry units, Part 4: Preformed foam cellular concrete blocks," New Delhi, India., 2008.

[38] "RILEM FMC-50:Determination of the fracture energy of mortar and concrete by means of three - point bend tests on notched beams," *Mater. Struct.*, vol. 18, no. 4, pp. 287–290, 1985.

[39] "BS EN 14651:2005. Test method for metallic fibred concrete. Measuring the flexural tensile strength (limit of proportionality (LOP), residual)," 2005.

[40] "JAPAN CONCRETE INSTITUTE: Method of test for fracture energy of concrete by use of notched beam (JCI-S-001-2003)."

[41] A. P. Fantilli, H. Mihashi, and P. Vallini, "Post-peak behavior of cement-based materials in compression," *ACI Mater. J.*, vol. 104, no. 5, pp. 501–510, 2007.